Title
AUTONIZATION OF HIGHLY EXCITED Ar+ IONS PRODUCED BY ELECTRON IMPACT

Authors
Newton, Amos S.
Sciamanna, A.F.
Clampitt, R.

Publication Date
1967-05-01

UCRL-17546

cy. 2

University of California

Ernest O. Lawrence Radiation Laboratory

AUTOIONIZATION OF HIGHLY EXCITED Ar^+ IONS PRODUCED BY ELECTRON IMPACT

Amos S. Newton, A. F. Sciamanna, and R. Clampitt

May 1967

Berkeley, California

DISCLAIMER

To be submitted to J. Chem. Phys.

UCRL-17546
Preprint

UNIVERSITY OF CALIFORNIA

Lawrence Radiation Laboratory
Berkeley, California

AEC Contract No. W-7405-eng-48

AUTOIONIZATION OF HIGHLY EXCITED Ar^+ IONS PRODUCED BY ELECTRON IMPACT

Amos S. Newton, A. F. Sciamanna, and R. Clampitt

May 1967

AUTOIONIZATION OF HIGHLY EXCITED Ar^+ IONS PRODUCED BY ELECTRON IMPACT*

Amos S. Newton, A. F. Sciamanna, and R. Clampitt

Lawrence Radiation Laboratory
University of California
Berkeley, California

May 1967

ABSTRACT

The $(M/q)^* = 10$ peak in the mass spectrum of argon observed at ionizing electron energies of 40 to 120 eV (uncorr.), is shown to consist of approximately equal contributions from: 1) surface-induced transitions of an excited Ar^+ ion to Ar^{++} at the last ion-source slit, and 2) an autoionization of an excited Ar^+ ion after the last ion-source slit. By use of an auxiliary slit beyond the last normal ion-source slit, these two processes were separable, and it is shown that the excited state undergoing surface-induced transitions is a different state than that undergoing autoionization, with the autoionizing state having an A.P. of 0.5 ± 0.2 eV higher than the state undergoing surface-induced transitions. The existence of autoionizing states of Ne^+ and Ar^{++} was also confirmed.

INTRODUCTION

In a recent paper[1] we confirmed the existence of highly excited states of noble gas ions and showed that they undergo transition to the next higher charge state near a metal surface. Excited states of Ar^+ were shown, in a Dempster type mass spectrometer, to undergo the transition:

$$(Ar^+)^* \xrightarrow{\text{Surface}} Ar^{++} + e^- \quad , \tag{1}$$

at the Isatron ion-source first slit, S_1, focus slit, S_F, and last slit, S_2. The assignment of the mass peak in argon which appears at an apparent mass $(M/q)^* = 10$ to the surface-induced transition at the last ion-source slit was, however, open to question, as Daly[2] has proposed the $(M/q) = 10$ peak in argon to be due to autoionization of an excited argon ion after the last ion-source slit of his mass spectrometer:

$$(Ar^+)^* \xrightarrow{\text{autoionization}} Ar^{++} + e^- \quad . \tag{2}$$

The experiments previously described[1] did not allow one to distinguish whether the $(M/q)^* = 10$ peak in argon arose by mechanism (1) or (2) or a combination of both. Previous work by McGowan and Kerwin[3] indicated the $(M/q)^* = 10$ peak in argon to arise from a collision-induced transition in the gas phase:

$$(Ar^+)^* + Ar \longrightarrow Ar^{++} + Ar + e^- \quad . \tag{3}$$

Kupriyanov and Latypov[4] found this peak in argon to arise both from a gas phase collision-induced process and a surface-induced transition at the last slit. Daly,[2] however, showed that, in his apparatus, the $(M/q)^* = 10$ peak of Ar was linear with ion-source pressure indicating the occurrence of either reaction (1) or (2). He obtained a half life of 0.8×10^{-6} sec for the process and concluded that it was one of auto-ionization.

In the present work, we show the $(M/q)^* = 10$ peak of argon, as observed with our apparatus, to be composed of two components of approximately equal intensity. One is due to a surface-induced transition at the last slit in the ion source and the other is due to autoionization. We are also able to show that these two components arise from different excited states of Ar^+.

EXPERIMENTAL METHOD

The work described here was performed on a Dempster type mass spectrometer (Consolidated Electrodynamics Corporation Model 21-103B). Most of the modifications have been described previously,[1] but some further modifications were necessary for the present investigation. The Isatron ion-source was modified by the addition of slit S_3 as shown in Fig. 1. The previously grounded last slit, S_2, was insulated from ground with alundum insulators. Slit S_3 was added using alundum spacers and insulators and was grounded. A separate lead was attached to slit, S_2, and this could be connected to ground or any one of a number of voltage points in the high voltage dropping resistor chain or in the mass marker resistor chain. In this way various voltages could be applied to S_2 up to a voltage of 0.069 V_A,

and these voltages were each proportional to the accelerating voltage, V_A. Higher voltages than 0.069 V_A could be applied to slit S_2, but small additional steps were attainable only by modifying the resistor chain. Since 0.069 V_A gave adequate separation of the peaks at $(M/q)^* = 10$ and there is considerable loss in intensity of all peaks with increasing V_{S_2}, further increases were deemed unnecessary. Three modifications of slit S_3 were used. 1) a slit 0.76 mm wide in a plate of 0.76 mm thickness, 2) the same slit increased in width to 1.0 mm, and 3) a slit 1.5 mm wide in a plate of thickness 0.76 mm with the slit opening covered on the side facing slit S_2 by a gold screen of ~82% transparency.

The inner focus control was increased in sensitivity by changing the existing 2.5 megohm potentiometer to a 0.5 megohm 10-turn potentiometer which could be inserted by a switch into any 0.5 megohm section of a total resistor string of 2.5 megohms. Focus plate voltages were measured with a Fluke null voltmeter. Scanning with the inner focus voltage was accomplished by using a motor drive on the 10-turn potentiometer.

The detector sensitivity was increased by about a factor of 40, (to approximately 10^{-15} A per chart division) with a gain in signal-to-noise ratio of about 20, by substituting a Loenco (Loe Engineering Co.) Model 21B electrometer for the existing amplifier on the mass spectrometer. A 10^{12} ohm grid resistor and a 1 mV recorder were used with this amplifier. Considerable increase of time constant in the recording system resulted from this change; therefore, the scanning speed was reduced by a factor of about 60 by use of a 2×10^9 ohm resistor in the voltage scanning circuit. At this scanning speed, peaks were recorded with intensities greater than 95% of their steady state intensities.

Owing to the slow rate of data collection using this amplifier, in order to keep a constant pressure in the apparatus, a 50 liter inlet volume was provided. The rate of leak from this volume was approximately 1% per hour.

EXPERIMENTAL RESULTS

When a potential is applied to slit S_2, an Ar^{++} ion from Eq. (1) will appear at an apparent mass given by[1]:

$$(M/q)^* = \frac{M(q_1V_1 + q_2V_2)}{q_2^2(V_1 + V_2)} \quad , \qquad (4)$$

where q_1 and V_1 are respectively the charge and accelerating potential of the ion before the transition, and q_2 and V_2 are the charge and accelerating potential of the ion after the transition. In Fig. 2 are shown the mass peak profiles in the region of $(M/q)^* = 10$ as observed under various conditions of S_2 and S_3. In Fig. 2A, where $V_{S_2} = 0.058\ V_A$ and S_3 is the gold screen, three peaks are apparent: one at $(M/q)^* = 10.00$, one at $(M/q)^* = 10.10$, and one at $(M/q)^* = 10.58$, plus a marked signal in the region between the 10.10 and 10.58 peaks. In Fig. 2B, where S_3 is an open slit, the peaks are the same except that the peak at 10.00 is reduced to a shoulder on the $(M/q)^* = 10.10$ peak. When S_2 is grounded (Fig. 2C) all these are consolidated into a single peak of $(M/q)^* = 10.02$. All peak masses were measured at the peak maximum with a precision of ±0.01 amu with respect to the mass scale calibrated at $Ar^{+++} = 13.33$.

In Fig. 3, the mass positions of these peaks are shown as a function of the voltage on slit S_2. The open circles are for an open slit at S_3; the position of the shoulder on the residual peak near $(M/q)^* = 10$ is not shown. Each point is the average of 4 to 6 measurements which differed in value by less than $\pm$ 0.01 mass units. The solid points were measured with the gold screen at S_3. The solid lines A and C are calculated from Eq. (4), for surface-induced transitions at slits S_2 and S_3 respectively. The intermediate points on dashed curve B for the second peak in Fig. 2A show this peak to increase in apparent mass from 10.02 (sum of all peaks) at $V_{S_2} = 0$, to 10.12 at $V_{S_2} = 0.069\ V_A$, the increase being linear with V_{S_2}.

A self-consistent interpretation of this data can be made if it is assumed that both processes (1) and (2) contribute. In Fig. 2A, with S_3 the gold screen, the peaks at $(M/q)^* = 10.00$ and 10.58 are due to surface-induced transitions at slits S_3 and S_2 respectively, the peak at $(M/q)^* = 10.10$ is due to autoionization after slit S_3, and the signal observed between $(M/q)^* = 10.10$ and 10.58 is due to autoionization in the space between S_2 and S_3. The behavior of the peak at $(M/q)^* = 10.58$ (Fig. 2A, 2B) with voltage on slit S_2, as shown in Fig. 3, proves that this peak arises at slit S_2, while the lack of such an effect in the $(M/q)^* = 10.00$ peak and the drastic reduction in its intensity when S_2 is changed to an open slit show this latter peak to arise at S_3. The movement in mass position of the $(M/q)^* = 10.10$ peak in Fig. 2A and 2B with V_{S_2} can be qualitatively understood on the basis of the ion optics of autoionization after acceleration in a Dempster type instrument and is discussed later in this paper.

In Fig. 4, the effect of pressure on the peaks of Fig. 2B and 2C are shown. The peak intensities are essentially linear with pressure and also with electron current from 5 to 80 μA; hence they arise from first order or pseudo-first order mechanisms. The observed abundances are critically dependent on the focusing characteristics and space charge densities in the ion-source, so for each measurement it was necessary to readjust the inner focus potential for maximum signal at the collector.

The focus conditions of these respective peaks is especially illuminating. First, because the magnetic field, H, and the accelerating voltage, V_A, are set to collect $(M/q)^*$ = 10 when its production depends upon M/q = 40 being focused at S_2, the ratio of inner to outer focus voltage is quite different than if H and V_A were set to collect M/q = 40. This situation arises because, in a Dempster type instrument, the ion-source is in the magnetic field and thus acts as a mass spectrometer of low resolution.

Under normal conditions of operation with S_2 grounded, and the potentials on the focus slit adjusted for maximum peak intensity and minimum beam width at the collector, the focal point of the lens system S_1-S_F-S_2 is at slit S_2. When S_2 is operated at a potential above ground with no change in V_F, the decrease in field gradient between S_F and S_2 increases the focal length of the lens system and the focal point is beyond S_2. At a given voltage on S_2 however, the potential on S_F can be changed to again make the focal point of the lens system at S_2. In Fig. 5, with V_{S_2} = 0.069 V_A, are shown superimposed tracings of the intensity profiles of the $(M/q)^*$ = 10.12 peak (dashed line) and the $(M/q)^*$ = 10.69 peak (solid line) obtained by scanning the ion beam across slit S_2 with the inner focus

voltage for four separate values of the outer focus voltage. With a high field gradient between S_1 and S_F, where the focal point is well beyond S_2, (curve A) the two profiles are similar but with a distinct broad maximum in the center of the M/q = 10.69 peak profile. At a lower field gradient, (curve B), the maximum in the center of the 10.69 peak profile is quite sharp while the 10.12 peak profile is symmetrical. At still lower field gradients, (curves C and D), the 10.69 peak is split into two sections and the 10.12 peak is centered over the minimum between the two. These curves conclusively prove that the peak at $(M/q)^* = 10.69$ arises from the Ar^+ ion beam striking the slit edges of S_2, while the peak at $(M/q)^* = 10.12$ arises from Ar^+ passing through slit S_2. In Fig. 5D, the Ar^+ beam is well focused at S_2 and has a beamwidth at S_2 narrower than the slit. Thus as the Ar^+ beam is scanned across the slit, the $(M/q)^*=10.69$ peak intensity rises as the beam impinges on the first slit edge, reaches a maximum as it crosses this slit edge, then decreases to a minimum when essentially all of the beam is passing through the slit. As the beam crosses the other slit edge, the peak intensity rises to another maximum. The $(M/q)^*=10.12$ peak intensity has a single maximum when the beam is focused in the center of the slit. In Fig. 6 are shown the $(M/q)^* = 10$ peaks when scanned under the outer focus conditions of Fig. 5D. In Fig. 6A the inner focus is at the maximum of the 10.69 peak; in Fig. 6B the inner focus is at the minimum for the 10.69 peak and the maximum for the 10.12 peak. This illustrates the dependence of the peak intensities on very small changes of focus conditions and also facilitates at least a partial separation of the peaks produced by the two mechanisms.

In Fig. 6A and 6B, the ratio of the intensity of the shoulder on the 10.12 peak to its maximum peak height is constant as is the ratio of the rise between

the peaks (measured by the extrapolated rise at $(M/q)^* = 10.69$), to the maximum height of the 10.12 peak. Both these features are thus related to the beam intensity passing through S_2. We ascribe both to the autoionization process.

Ionization efficiency curves of these peaks have been obtained under various conditions of focus, with S_3 the gold screen, and with S_3 the open slit. Typical examples are shown in Fig. 7 for which the focus conditions were near those of Fig. 5B, i.e., a maximum for both the 10.10 and 10.58 peaks ($V_{S_2} = 0.058\ V_A$) at the same inner focus setting. Slit S_3 was the gold screen. In Fig. 7 are plotted the ionization-efficiency curves for the 10.00, 10.10 and 10.58 peaks with no correction for cross contributions to these respective peaks. The curves have been normalized to the peak maximum which occurs at an electron energy of 57.5 eV (uncorr.). The curves for the 10.00 and 10.58 peaks are seen to be essentially identical, and differ markedly from the curve for the 10.10 peak. Both sets of curves show a maximum at 57.5 eV (uncorr.) but the maximum of the 10.10 peak is sharper and this curve falls off much faster at higher electron energies. In addition, at lower electron energies, the curve for the 10.10 peak crosses over the curve of the other two peaks and extrapolates to a higher appearance potential. Values from six different sets of curves under various conditions of focus, pressure, and ion accelerating voltage all show the $(M/q)^* = 10.10$ peak to have an appearance potential 0.3 to 0.7 eV higher than that of the $(M/q)^* = 10.00$ and 10.58 peaks. We therefore estimate the difference in appearance potential of the states contributing to these two processes as 0.5 $\pm$ 0.2 eV.

In Fig. 7, it must be realized that there is a contribution from the 10.10 peak to the 10.00 peak and a contribution from the rise between the peaks to the 10.58 peak. We have no means of estimating whether or not the 10.00 peak contributes to the 10.10 peak intensity. These cross contributions will lower the high electron energy portions of the ionization efficiency curves for the 10.00 and 10.58 peaks. When the 10.58 peak is plotted as two separate components, i.e., the extrapolated rise between the peaks as measured at $(M/q)^*$ = 10.58, and the residual peak above this rise, then at high electron energies the curve for the residual 10.58 peak is raised, while the curve for the extrapolated rise is identical, within experimental error, with that of the $(M/q)^*$ = 10.10 peak.

The curve for the M/q = 10.10 peak is similar to that given by Daly[2] for his $(M/q)^*$ = 10 peak which was ascribed to autoionization of an excited state of Ar^+. We conclude that the $(M/q)^*$ = 10.10 peak is the result of an autoionization process. We further conclude that the 10.00 and 10.58 peaks arise from surface-induced transitions at S_3 (gold screen) and slit S_2 respectively and that the excited state (or states) of Ar^+ undergoing surface-induced transitions is different from the excited state undergoing autoionization.

We have not made detailed studies on other noble gases and higher charged states of argon, but have qualitatively looked at $(He^+)^*$, $(Ne^+)^*$, $(Ar^{++})^*$ in regard to surface-induced transitions at S_2 and S_3 compared to autoionizations.

In helium no peak at $(M/q)^*$ = 1 was observed at the highest sensitivity and at high pressures. Inasmuch as the transition:

$$(He^+)^* \xrightarrow{S_F} He^{++} + e^- \qquad (5)$$

at the focus slit was seen previously,[1] it is expected that surface-induced transitions at S_2 and S_3 should occur. However an autoionizing state is manifestly impossible in a one-electron atomic system. In $(Ar^+)^*$, the maximum ratio of the intensity of $(M/q)^* = 10$ to the intensity of the surface-induced peak at S_F was about 1:40. As has been shown in the present work, only about half the $(M/q)^*=10$ peak was surface-induced, so the ratio of conversion at slits S_2 and S_F respectively was actually about 1:80. Hence, judging from the intensities of the He^+ and Ne^+ surface-induced transition peaks at S_F,[1] no peak should be observable for the transition at S_2 or S_3 even at the highest sensitivity used. Therefore the absence of an observable $(M/q)^* = 1$ peak in He is most likely due to a lack of sufficient sensitivity in the detection system.

In Ne^+, an $(M/q)^* = 5$ peak is observed at high pressures. With V_{S_2} applied, the peak is seen to be essentially all due to an autoionization process occurring after S_3 and between S_2 and S_3, since it resembles that of $(Ar^+)^*$ when focused to minimize the surface-induced components (Fig. 6B). A similar situation was found for the $(M/q)^* = 8.9$ peak from $(Ar^{++})^*$. Here again only the autoionization peak was seen but the aforementioned intensity considerations suggest that the yield from surface-induced transitions at S_2 or S_3 will also be too low to observe with the present apparatus.

In krypton and xenon, the multiplicity of isotopes makes it impossible to achieve a separation for any one isotope of the S_2 and S_3 surface-induced

and autoionization peaks without overlapping the set of peaks from another isotope. With mono-isotopic Kr and Xe this method should separate the components arising from the two mechanisms.

DISCUSSION

The results presented here show that with the apparatus used in this investigation, the $(M/q)^* = 10$ peak of argon observed at ionizing electron energies of 40 to 120 eV is the result of the sum of two processes. The first process is the surface-induced transition of $(Ar^+)^*$ to Ar^{++} at the last slit of the ion source, Eq. (1). Second is a transition which satisfies all criteria for an autoionization and we agree with Daly that this is an autoionizing process. Further, we conclude that these two transitions occur from different excited states of the argon ion, the autoionizing state having an appearance potential 0.5 ± 0.2 eV higher than that of the state undergoing surface-induced transitions.

For autoionization to occur, the total energy of excitation of Ar^+ must be greater than the ionization potential of Ar^+, i.e., the excited state must lie above the ground state of Ar^{++}. Such a state could be one in which two of the five remaining 3p outer electrons in Ar^+ are each excited to higher levels, the total energy of the excitation being greater than the ionization potential of Ar^+. A second possibility is the excitation of an inner 3s electron to a higher state, and when the return transition occurs, ionization occurs by an Auger process. In the absence of data on the energy levels of the inner electrons in Ar^+, a specific assignment does not appear feasible at present.

From the shapes of the ionization efficiency curves, both have the appearance of resonance processes but the slower falloff with increasing electron energy beyond the maximum at 57.5 eV of the surface-induced peak intensity suggests that the excitation bandwidth of the states undergoing surface-induced transitions is greater than the bandwidth of those undergoing autoionization.

If the $(M/q)^*$ = 10.12 pk at V_{S_2} = 0.069 V_A is to be ascribed to autoionization of $(Ar^+)^*$ to yield Ar^{++} in the free space beyond slit S_3, then the increase in apparent mass of this peak with increasing V_{S_2} must be explained. Coggeshall[5] and Newton[6] have given following the equation for the apparent radius (related to apparent mass) of the product ion of a metastable transition as a function of distance traveled by the parent ion after acceleration in a Dempster type mass spectrometer:

$$r^* = \frac{(R-r)^* + r^2 - R(2r-R)\ \cos\theta}{R + (2r-R)\ \cos\theta} \quad , \qquad (6)$$

where R is the radius of the parent ion under the conditions of V_A and H for collecting the daughter ion, r is the radius of normal ion trajectory, and θ the angle through which the parent ion travels in its trajectory of radius R before the transition.

For the autoionization of $(Ar^+)^*$,

$$(Ar^+)^* \longrightarrow Ar^{++} + e^- \quad , \qquad (7)$$

if $(M/q)^*$ = 10 is to be collected, then R, the radius of $(Ar^+)^*$ will be equal to 2r. Therefore in Eq. (6) the coefficients of cos θ are zero (2r = R) and r^* will always be equal to r. Hence there is no change in apparent mass with distance beyond the ion source at which the transition occurs.

However, Eq. (6) was derived on the implicit assumption that the parent ion emerges from the ion source in a trajectory normal to the plane of the last slit. If however, the parent ion emerges from the last slit at an angle ϕ with respect to the normal, then the situation is more complicated and Eq. (6) no longer adequately describes the situation. Figure 8 shows the schematic representation of the metastable ion trajectories for the case in which ϕ is toward the magnet center. Under these conditions the equation for r^*, the apparent radius at which the daughter ion is collected and g, the displacement of the new center from the normal center C_o are given by the equations[7]:

$$r^* = \frac{R^2 + 2r^2 - R^2 \text{Cos}\ \theta + 2\ Rr\ \text{Cos}\ (\theta+\phi) - 2Rr\ \text{Cos}\ \phi}{R + 2r\ \text{Cos}\ (\theta+\phi) - R\ \text{Cos}\ \theta} \tag{8}$$

$$g = (R-r^*)^2 + R^2 + r^2 - 2\ Rr\ \text{Cos}\ \phi - 2r(R-r^*)\text{Cos}(\theta+\phi) - 2R(R-r^*)\text{Cos}\ \theta \tag{9}$$

When $\phi = 0$, these equations become identical with Eq. (6). When ϕ is away from the magnet center (designated as ϕ = negative in Figs. 9 and 10), the same equations apply except that where $(\phi+\theta)$ occurs in Eqs. (8) and (9), one substitutes $|\theta-\Phi|$.

As previously shown,[5,6] peak cutoff occurs when: 1) $r^* + g$ is equal to the outer radius of the analyzer tube, i.e., the outer cutoff, and 2) $r^* - g$ is equal to the inner radius of the analyzer tube, the inner cutoff.

In Fig. 9, the field of collectable orbits for the autoionization of $(Ar^+)^*$ to Ar^{++} as a function of ϕ and θ is plotted. The upper and lower solid lines

represent the outer and inner tube cutoffs respectively. The dashed lines are isobars of the labeled apparent masses. An absolute cutoff of this whole field occurs at about $\phi = 18°$ where the $(Ar^+)^*$ ion strikes the inner surface of the analyzer tube. The angle θ through which orbits are collectable is directly related to the distance of travel over which dissociation can occur, i.e., related to the time available for dissociation, hence the intensity of the resulting peak. In the region of $\phi = 0$, the peak is centered around $(M/q)^* = 10.00$, and with the normal $\pm 2°$ spread in angle of emergence from slit S_2, the limits are from 9.95 to 10.05. As the spread in ϕ increases, those deviations away from the magnet center (ϕ designated as negative) have only a small range of θ of collectable orbits and therefore contribute less to the peak intensity than do deviations toward the magnet center (ϕ designated as positive) where the range of θ of collectable orbits is larger. As ϕ increases more orbits of apparent mass greater than 10.00 are collected and the integrated apparent mass increases. In Fig. 10, is shown the distance traveled in collectable orbits (dashed line) and the average apparent mass of these orbits as a function of ϕ. It is seen that in order for the average apparent mass to be 10.1, the angle of deviation must be about 6° toward the magnet center.

Such deviations in ϕ can occur because: 1) the trajectory of $(Ar^+)^*$ through S_2, under conditions when V_A and H are set to focus M/q = 10 at the collector, is normally at a slight angle toward the magnet center since the $(Ar^+)^*$ beam has been forced through S_2 (when normally (M/q) = 10 should be focused through S_2) by changing the relative potentials on the inner and outer focus plates; 2) when S_2 is above ground potential, the S_2 - S_3 slit system becomes a slightly divergent lens. The ion optics of this system

(in combination with the S_1-S_F-S_2 lens system) is complicated and has not been calculated, but qualitatively it is clear that the divergence of an ion is proportional to both the voltage gradient between S_2 and S_3 and the initial angle of divergence through S_2. Both the gradient between S_2 and S_3 and the focal point of the S_1-S_F-S_2 lens system change with V_{S_2}.

One may thus qualitatively understand the peak distribution in Fig. 2. In Fig. 2A the surface-induced transitions at S_3 giving the 10.00 peak, all occur near $\theta = 0$ (actually $\theta = 0.47'$ of arc from S_2) and Fig. 9 shows that such transitions will all give apparent masses between 9.95 and 10.00 (curve C of Fig. 3). The surface-induced transitions at S_2, $(M/q)^* = 10.58$ in Fig. 2A, also occur with $\theta = 0$ by definition of θ, and hence appear at the mass calculated from Eq. (4). The peak due to autoionization will, however, be displaced at high V_{S_2} values owing to the increased contribution of Ar^{++} ions arising at higher ϕ and θ values which correspond to greater apparent masses. In Fig. 2B, the shoulder probably arises from those ions emerging normally from S_2 and hence are not appreciably deflected by the field between S_2 and S_3. The peak at $V_{S_2} = 0$ in Fig. 2C, with an apparent mass of 10.02, indicates that most of the beam through S_2 is within a spread of less than 2 or 3° deflection from a normal trajectory.

ACKNOWLEDGMENT

The authors wish to thank Joan Delmonte for making many of the calculations on which Fig. 9 is based.

Footnotes and References

*This work was performed under the auspices of the U. S. Atomic Energy Commission.

1. A. S. Newton, A. F. Sciamanna, and R. Clampitt, J. Chem. Phys. 46, 1779 (1967).

2. N. R. Daly, Proc. Phys. Soc. (London) 85, 897 (1965).

3. J. Wm. McGowan and L. Kerwin, Can. J. Phys. 41, 1535 (1963).

4. S. E. Kupriyanov and Z. Z. Latypov, Soviet Physics JETP 20, 36 (1965).

5. N. D. Coggeshall, J. Chem. Phys. 37, 2167 (1962).

6. A. S. Newton, J. Chem. Phys. 44, 4015 (1966).

7. Eqs. (8) and (9) are only very close approximations since the variation of R with r^* has not been considered. As the accelerating voltage, V_A, or the magnetic field, H, is adjusted to collect an ion of apparent radius, r^*, at the collector slit, a small change in R occurs. For the range of values of r^* considered in the present work, this correction is negligible.

Figure Captions

Fig. 1. Modified Isatron ion source. R = repellers, normally run at ~1.01 V_A; S_1 = ion source first slit, run at V_A; S_F = ion-source focus slits, normally run at ~0.92 V_A; S_2 = ion-source last slit, normally grounded but now insulated from ground and run at V_{S_2}; S_3 = added slit, run at ground potential.

Fig. 2. Peak profiles of $(M/q)^*$ = 10 peaks in argon using modified Isatron ion source.

A) Slit S_3 = gold screen, V_{S_2} = 0.058 V_A

B) Slit S_3 = 1.0 mm slit, V_{S_2} = 0.058 V_A

C) Slit S_3 = 1.0 mm slit, V_{S_2} = 0

conditions: inlet pressure = 1000μ, V = 57.5 eV, I = 75 μA, MV = 7540.

Peak intensities are on an arbitrary scale.

Fig. 3. Shift in apparent mass of $(M/q)^*$ = 10 peaks in argon with potential on slit S_2. Solid lines of curves A and C are calculated for surface-induced transitions at slits S_2 and S_3 respectively.

open circles - slit S_3 = 0.76 mm slit

solid points - slit S_3 = gold screen

Fig. 4. Linearity with pressure of the $(M/q)^*$ = 10 peaks in the mass spectrum of argon. The intensity of Ar^{+++} is used as the comparison standard. The ratio of ion source pressure to inlet system pressure = 8.6×10^{-4}.

A) $(M/q)^*$ = 10.00 , V_{S_2} = 0

B) $(M/q)^*$ = 10.04 , V_{S_2} = 0.0213 V_A

C) $(M/q)^*$ = 10.21 , V_{S_2} = 0.0213 V_A

Fig. 5. Variation in peak intensities of the autoionizing $(Ar^+)^*$ peak ($(M/q)^*$ = 10.12) dashed curves and the S_2 surface-induced transition peak ($(M/q)^*$ = 10.69) solid curves, as observed when the Ar^+ is scanned across slit S_2

by varying the inner focus potential at various designated values of the outer focus potential (O.F.).

Conditions: V_{S_2} = 0.069 V_A, Inlet pressure = 1000μ, I_{e^-} = 75 μA. V_{e^-} = 57.5 eV, MV = 7540, S_3 = 1.0 mm slit.

Fig. 6. Peak profiles of the $(M/q)^*$ = 10 peaks in argon at high outer focus voltage (Fig. 4D, O.F. = 0.952 V_A).

A) Inner focus set at the first maximum of the slit S_2 surface-induced peak.

B) Inner focus set at the center minimum of the slit S_2 surface-induced peak and the maximum of the peak due to autoionization.

Conditions: Inlet pressure = 1000μ, V_{e^-} = 57.5 eV, I_{e^-} = 75 μA, V_{S_2} = 0.069 V_A, MV = 7540, S_3 = 1.0 mm slit.

Fig. 7. Ionization efficiency curves for various components of the $(M/q)^*$ = 10 peak in argon. Open circles, $(M/q)^*$ = 10.00 peak from surface-induced transitions at slit S_3; solid circles $(M/q)^*$ = 10.58 peak from surface-induced transitions at slit S_2; and triangles, $(M/q)^*$ = 10.10 peak from autoionization of $(Ar^+)^*$ beyond slit S_3.

Conditions: Slit S_3 = gold screen, V_{S_2} = 0.058 V_A, MV = 7540, inlet pressure = 1000μ, I_{e^-} = 75 μA, repellers = 1.011 V_A.

Fig. 8. Schematic construction for deriving r^* and g as a function of R, r, θ, and φ.

R = radius of parent ion; r^* = apparent radius of daughter ion; r = normal radius of ions, S_2 = Isatron last slit, S_c = collector slit, g = displacement of new center, C_{r^*} from normal center, C_o; θ = angle of travel of parent ion, M_o, in trajectory of radius R before transition; φ = deflection of ion

beam M_o^+ from perpendicular at slit S_2. Construction shown is for deflections of ϕ toward the magnet center.

Fig. 9. Field of collectable orbits for the autoionization $(Ar^+)^* \longrightarrow Ar^{++} + e^-$ as a function of the angle ϕ of emergence of $(Ar^+)^*$ through slit S_2 and the angle θ of travel on the Ar^+ orbit before transition. Upper solid line is the outer cutoff by the analyzer tube, lower solid line the inner cutoff by the analyzer tube. Dotted lines are isobars of apparent mass, $(M/q)^*$, of the daughter (Ar^{++}) ions. ϕ-positive is for deflections toward magnet center, ϕ-negative is for deflections away from magnet center.

Fig. 10. Mean apparent mass (solid line) and maximum distance of travel before dissociation (dashed line) for the autoionization of $(Ar^+)^*$ to Ar^{++} as a function of ϕ, the angle of emergence of $(Ar^+)^*$ through the Isatron last slit.

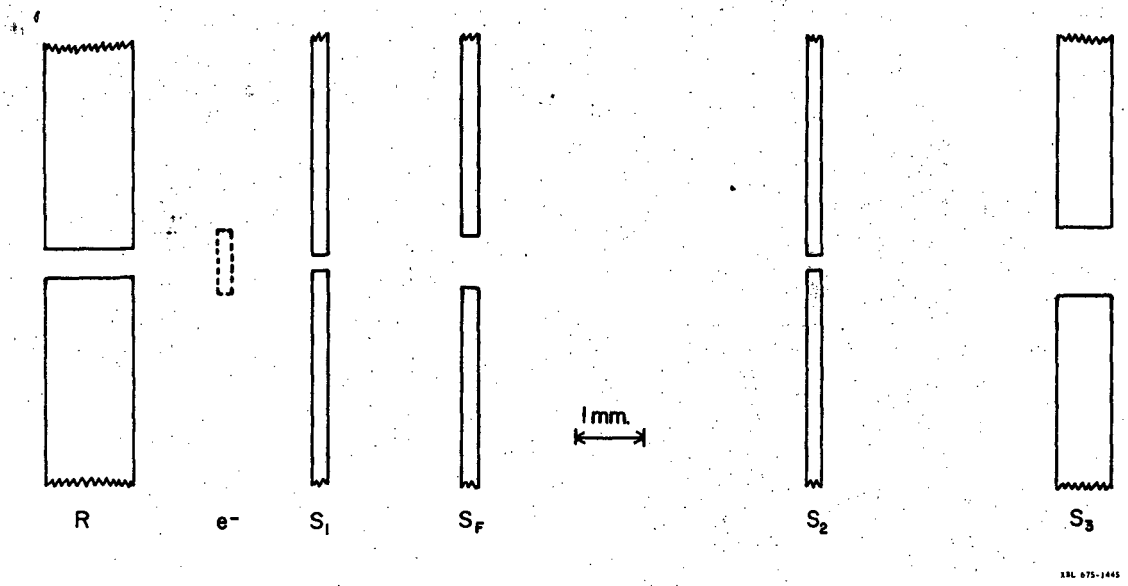

Fig. 1

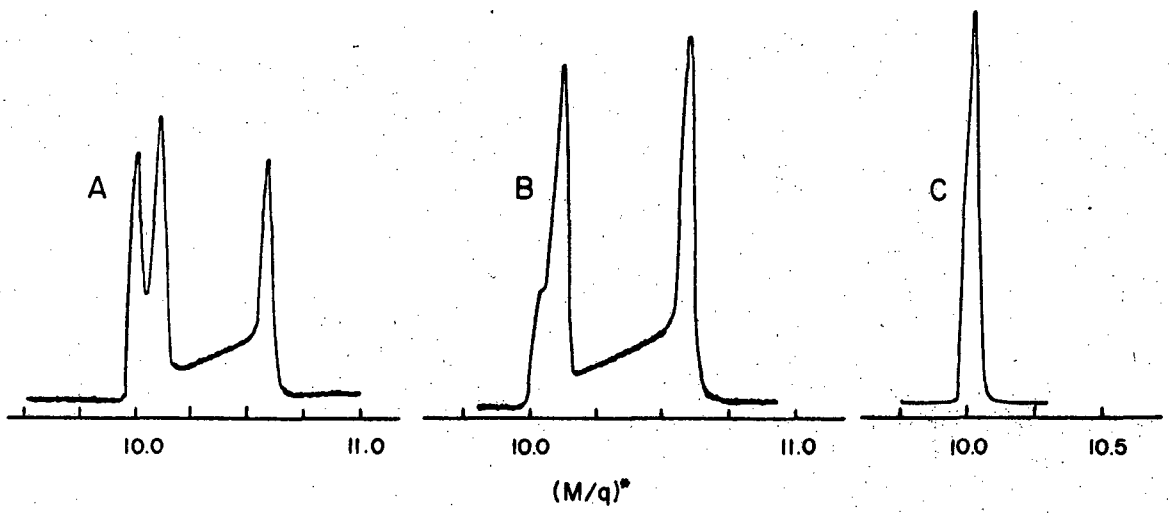

Fig. 2

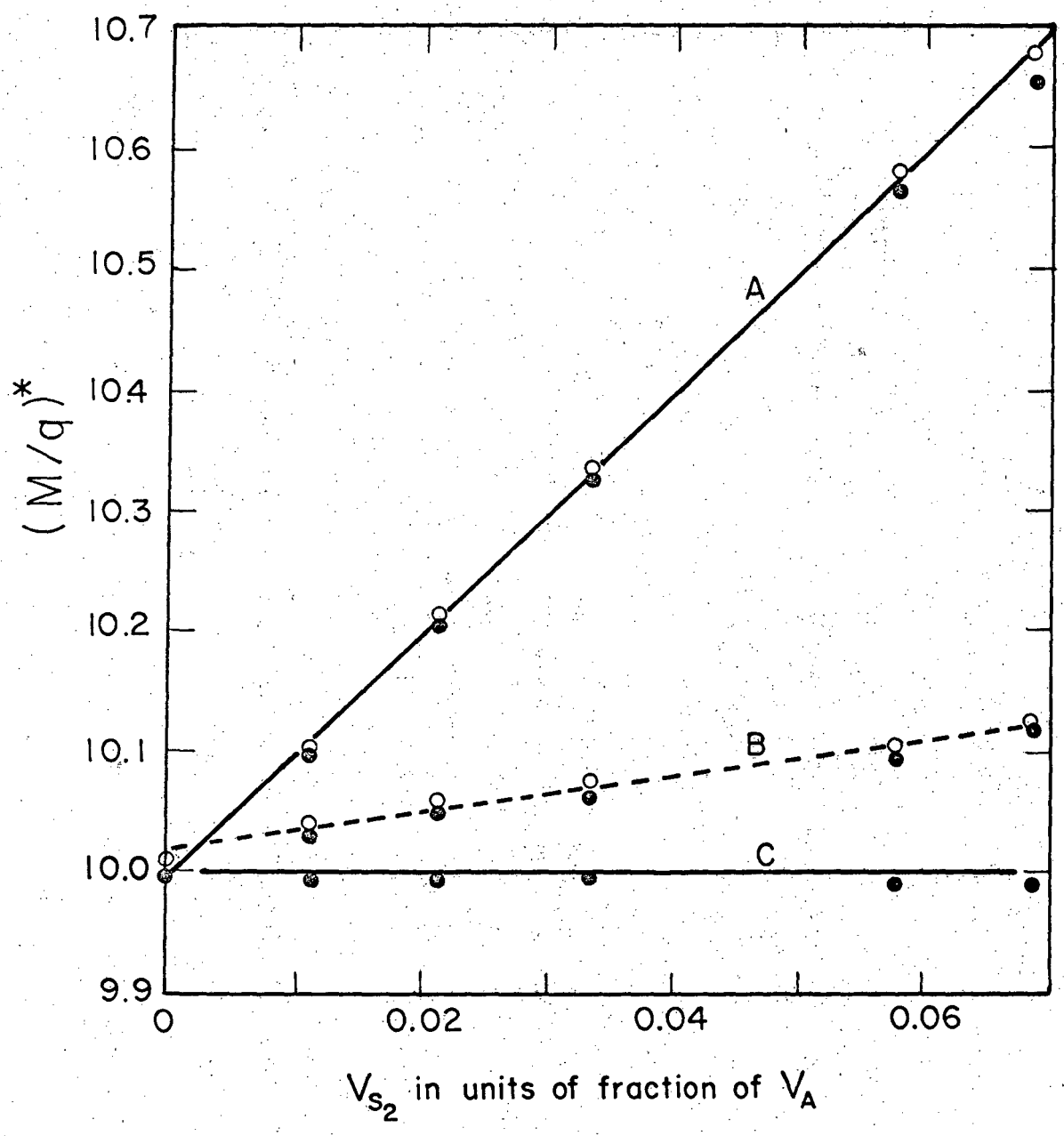
10.7
10.6
10.5
10.4
10.3
10.2
10.1
10.0
9.9
(M/q)*
A
B
C
0
0.02
0.04
0.06
V_{S_2} in units of fraction of V_A
XBL 675-1447

Fig. 3

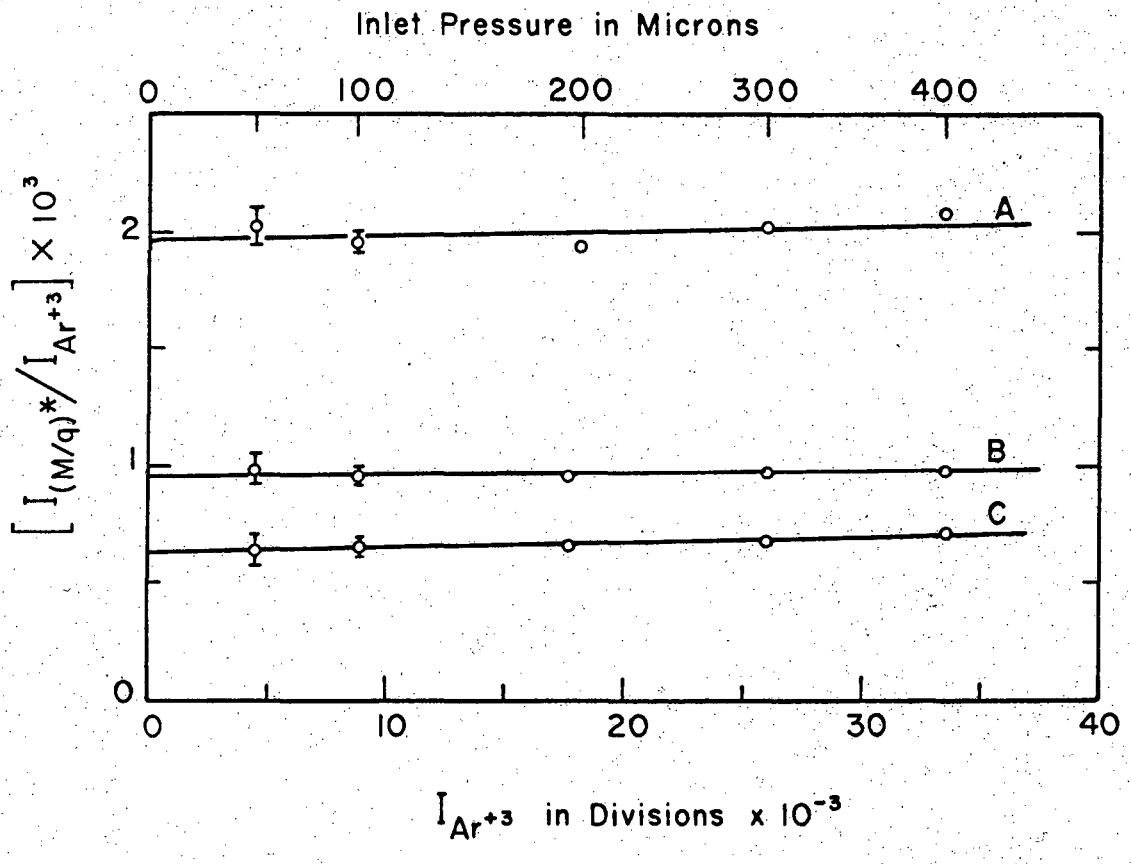

XBL 675-1448

Fig. 4

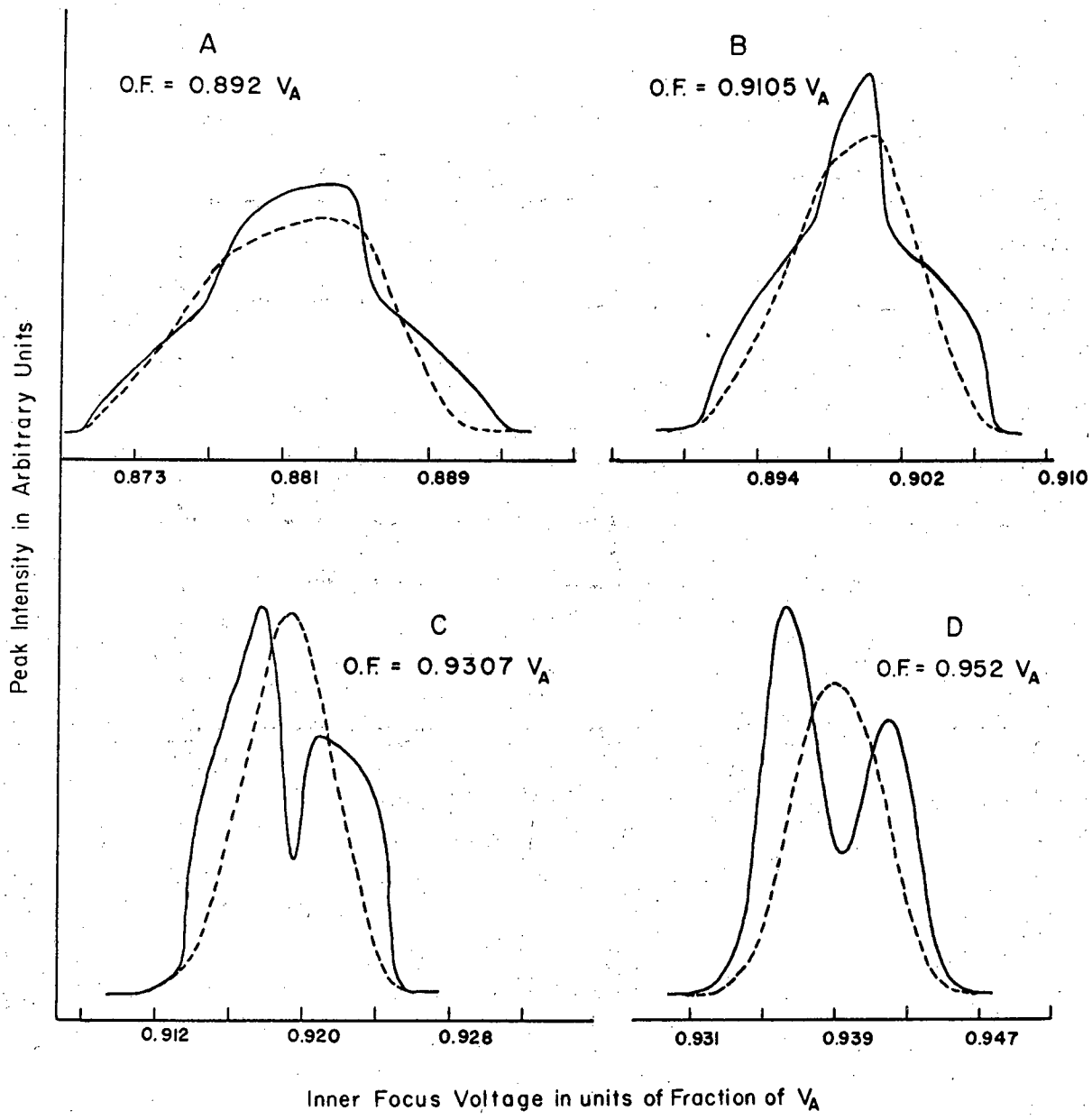
A
O.F. = 0.892 V_A
0.873
0.881
0.889
B
O.F. = 0.9105 V_A
0.894
0.902
0.910
C
O.F. = 0.9307 V_A
0.912
0.920
0.928
D
O.F. = 0.952 V_A
0.931
0.939
0.947
Peak Intensity in Arbitrary Units
Inner Focus Voltage in units of Fraction of V_A
XBL 675-1449

Fig. 5

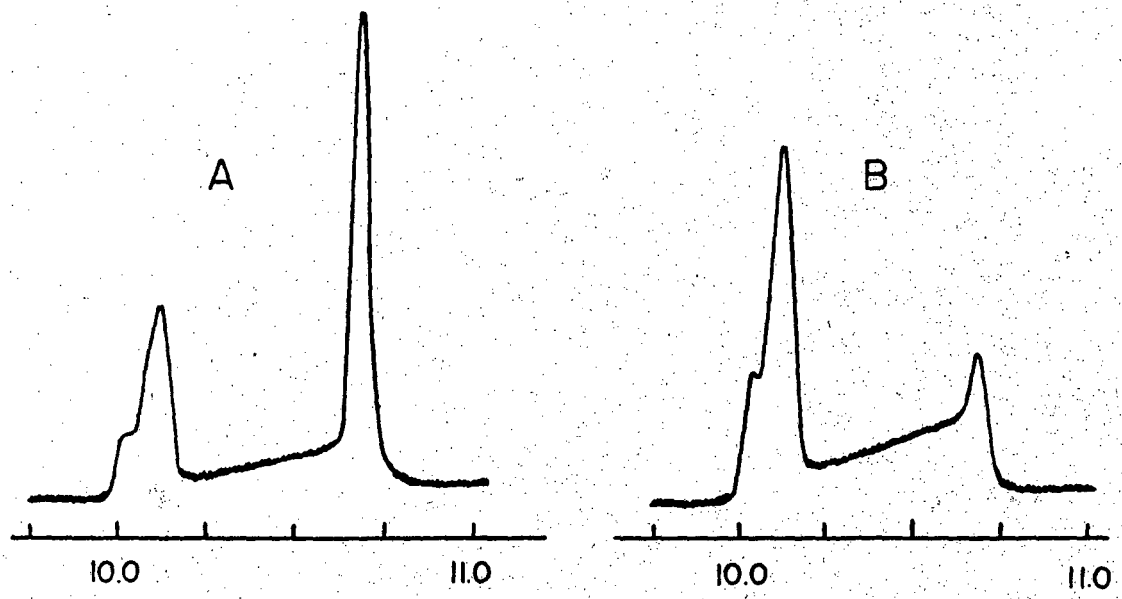

XBL 675-1450

Fig. 6

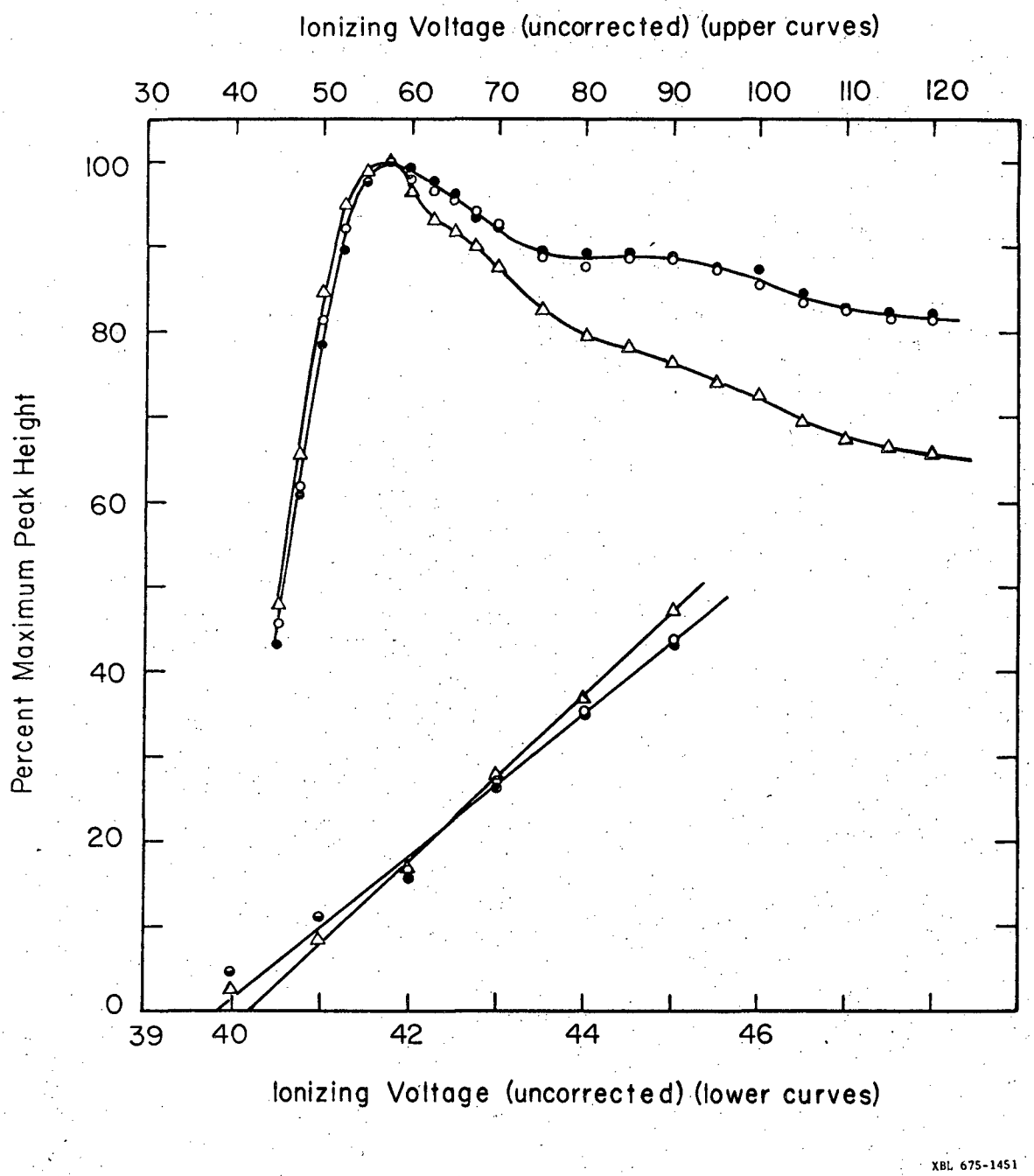

XBL 675-1451

Fig. 7

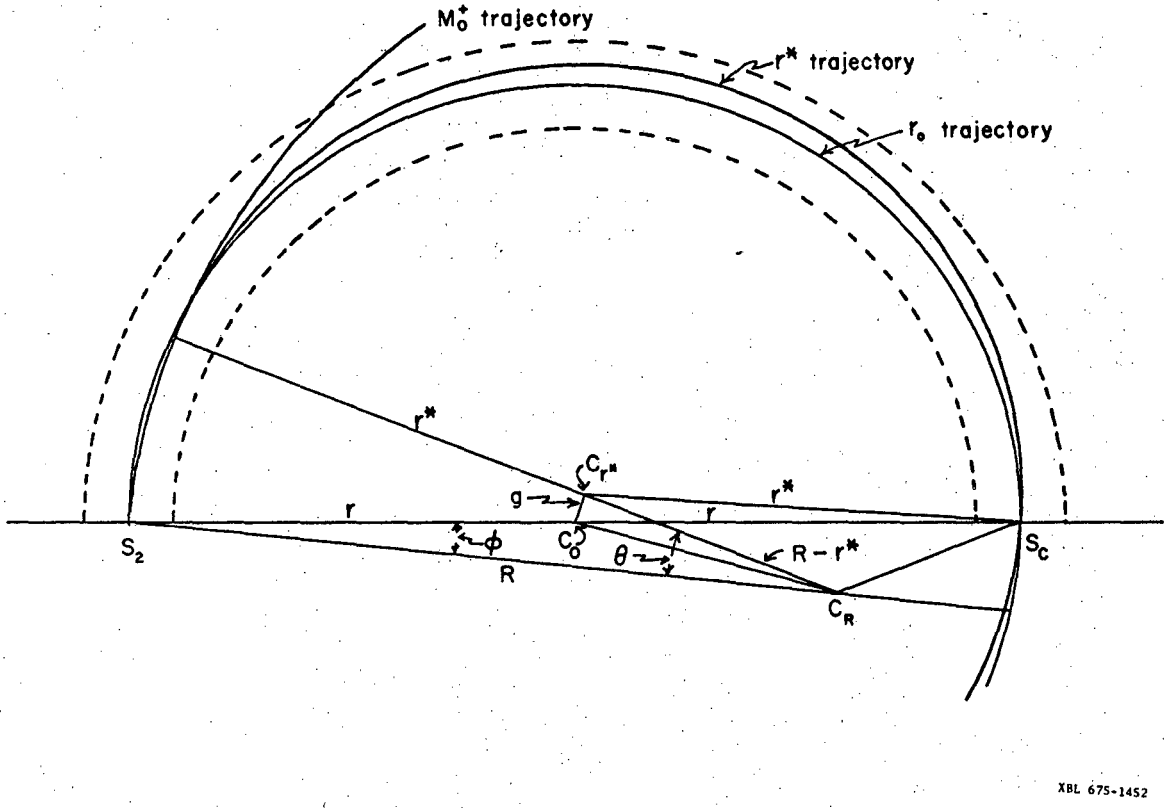
M_o^+ trajectory
r* trajectory
r_e trajectory
r*
C_{r^*}
g
r
r*
r
S_2
ϕ
R
C_o
θ
R − r*
S_c
C_R
XBL 675-1452

Fig. 8

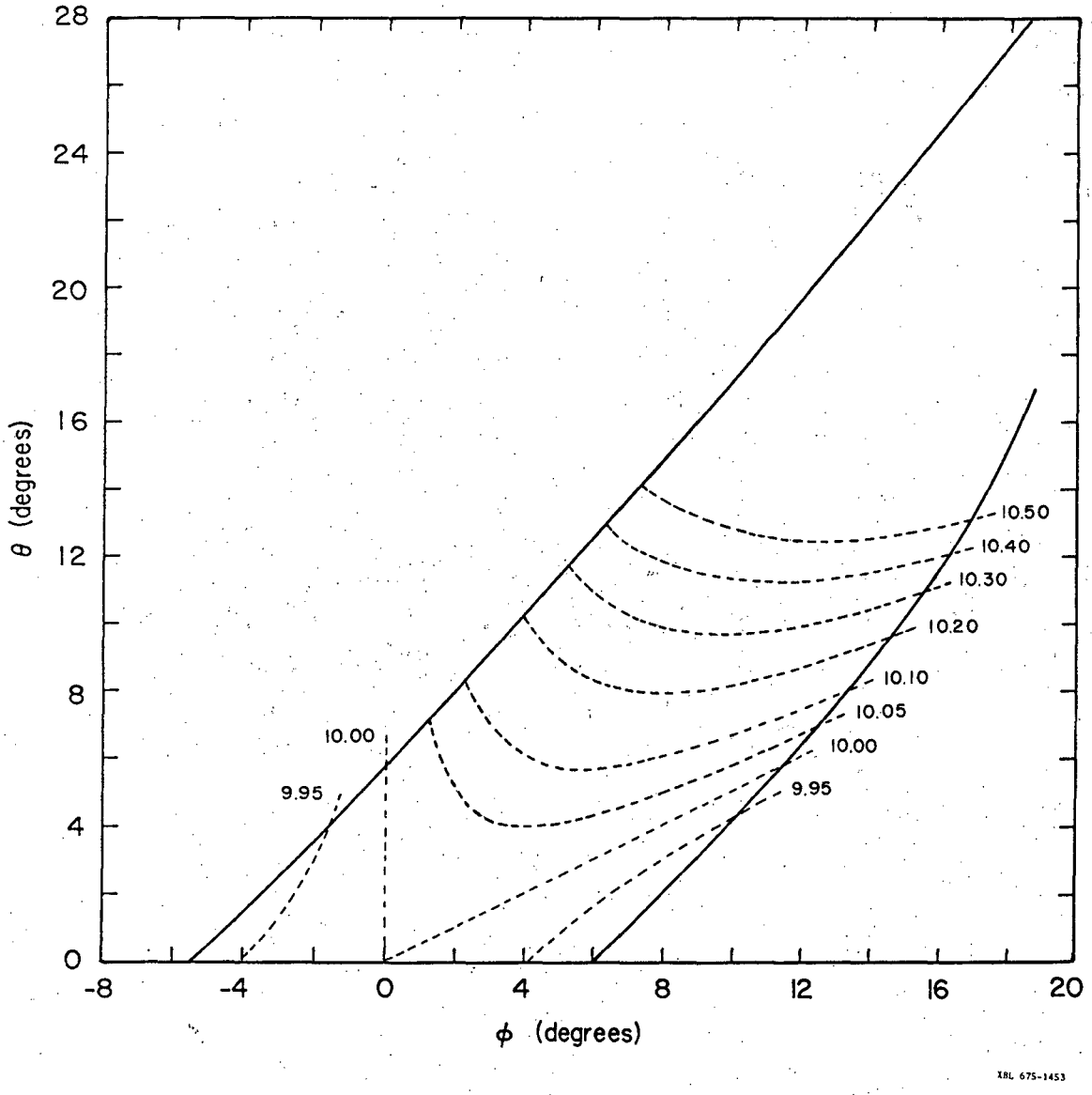
28
24
20
16
12
8
4
0
θ (degrees)
-8
-4
0
4
8
12
16
20
φ (degrees)
10.50
10.40
10.30
10.20
10.10
10.05
10.00
9.95
10.00
9.95
XBL 675-1453

Fig. 9

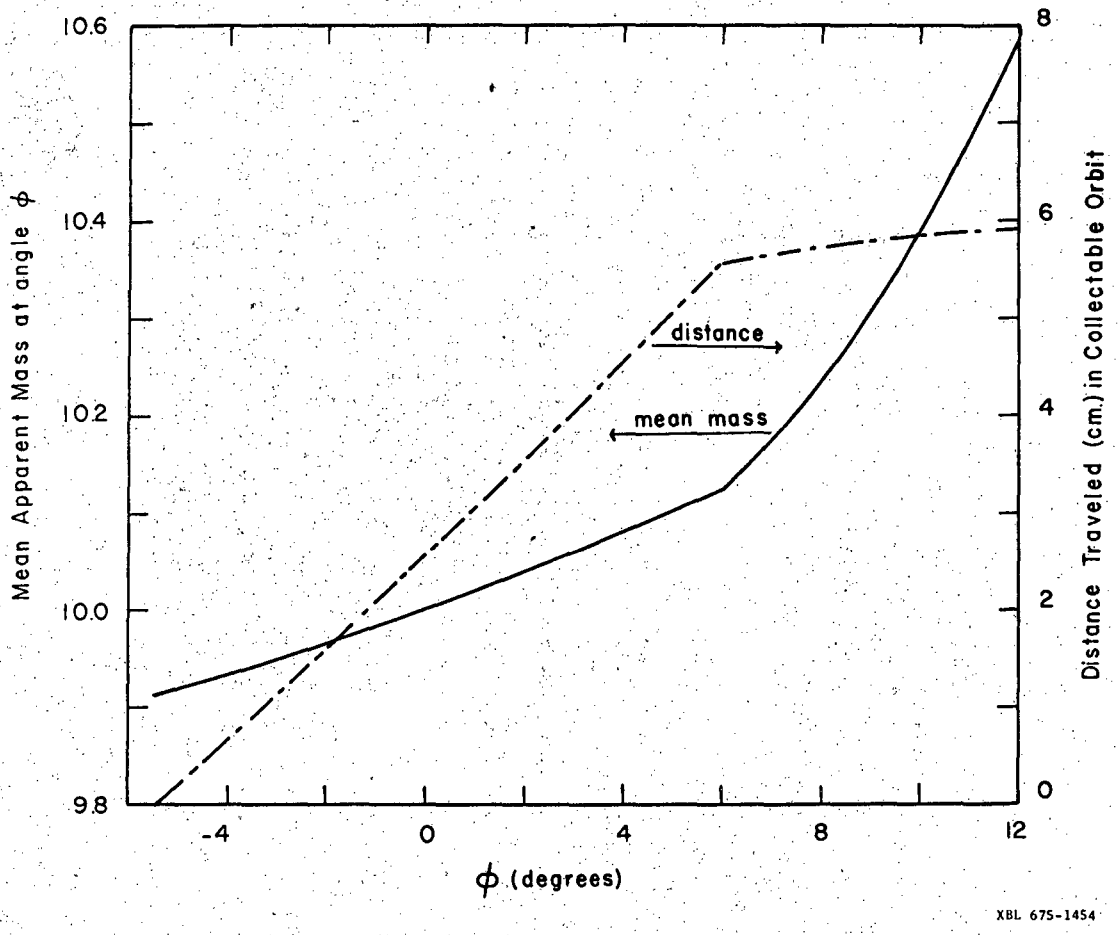
10.6
10.4
10.2
10.0
9.8
Mean Apparent Mass at angle φ
8
6
4
2
0
Distance Traveled (cm.) in Collectable Orbit
distance
mean mass
-4
0
4
8
12
φ (degrees)
XBL 675-1454

Fig. 10